Tuning polariton vortices in an asymmetric ring potential

Qiang Ai,[1] Xuekai Ma,[2] Franziska Barkhausen,[2,3] Xiaokun Zhai,[1] Chunzi Xing,[1] Xinmiao Yang,[1] Peilin Wang,[4] Tianyu Liu,[1] Yong Zhang,[4] Yazhou Gu,[5] Peigang Li,[6] Zhitong Li,[5] Zacharias Hatzopoulos,[7] Pavlos G. Savvidis,[8,9,7] Stefan Schumacher,[2,3,10] and Tingge Gao[1,*]

[1] *Department of Physics, School of Science, Tianjin University, Tianjin 300072, China*
[2] *Department of Physics and Center for Optoelectronics and Photonics Paderborn (CeOPP), Universität Paderborn, Warburger Strasse 100, 33098 Paderborn, Germany*
[3] *Institute for Photonic Quantum Systems (PhoQS), Paderborn University, Warburger Straße 100, 33098 Paderborn, Germany*
[4] *Center for Applied Mathematics and KL-AAGDM, Tianjin University, Tianjin, 300072, China*
[5] *State Key Laboratory of Information Photonics and Optical Communications, School of Science, Beijing University of Posts and Telecommunications, Beijing 100876, China*
[6] *School of Integrated Circuits & State Key Laboratory of Information Photonics and Optical Communications, Beijing University of Posts and Telecommunications, Beijing 100876, China.*
[7] *Institute of Electronic Structure and Laser (IESL), Foundation for Research and Technology-Hellas (FORTH), Heraklion 71110, Greece*
[8] *Key Laboratory for Quantum Materials of Zhejiang Province, Department of Physics, Westlake University, Hangzhou, Zhejiang 310024, China*
[9] *Institute of Natural Sciences, Westlake Institute for Advanced Study, Hangzhou, Zhejiang 310024, China*
[10] *Wyant College of Optical Sciences, University of Arizona, Tucson, AZ 85721, USA*

Exciton polariton condensates are macroscopic coherent states in which topological excitations can be observed. In this work, we observe the excitation of the vorices and realize tuning the topological charge by manipulating the pumping configurations. Using a digital micromirror device (DMD), we constructed an annular pumping pattern where the inner and outer rings can be easily tuned. Both the number and the topological charge of the vortices can be changed by slightly tuning the inner ring position against the outer ring. The experimental results can be reproduced in theory by the Gross-Pitaevskii (GP) equation. Our work offers to generate and manipulate vortices in exciton polariton condensates using a straightforward optical method.

A vortex typically can be observed with the phase winding of $2\pi n$ (where n is an integer, i.e., the topological charge) around a core along a closed path. This discrete phase accumulation forces the wave function's amplitude to drop to zero inside the core region enclosed by the path, thereby forming a localized singularity (vortex core) [1]. Vortices or vortex clusters can be observed in a wide range of physical systems [2–6], including Bose–Einstein condensation in cold atoms [7], superfluids [8], Abrikosov vortices in superconductors [9], Berezinskii–Kosterlitz–Thouless (BKT) transition in two-dimensional systems [10], and exciton polariton condensates [11]. Due to the tremendous potential applications such as topological quantum computing and optical communications[12–14], the generation and precise control of vortices have consistently been a central focus of research [15, 16]. Typically, the generation of vortices depends on external perturbations or fields [8, 17], whereas their control often relies on the introduction of specific structural defects or the use of pump light carrying orbital angular momentum to create a tailored optical field [18, 19]. However, these methods are limited by the complex structure design or pumping configurations.

Exciton polaritons are composite bosonic quasiparticles that emerge from the strong coherent coupling between excitons and photons in semiconductor microcavities [20, 21]. The small effective mass of exciton polaritons allows condensation at relatively high temperatures, even up to room temperature [22, 23], and the exciton component introduces a strong repulsive nonlinearity through exciton–exciton interactions [24–26]. Consequently, by designing appropriate potential traps, it is feasible to drive the formation of condensates and precisely control their modes [27–29]. Recently, this method has been widely applied to vortex generation and control [30–33].

In this work, we experimentally generate vortices in a planar semiconductor microcavity using only a simple annular nonresonant pumping pattern. By tuning the pumping configuration, we construct an annular exciton polariton potential resonator as sketched in FIG. 1(a). When the pump density is above the threshold, an exciton polariton condensate is generated within the resonator. The pump region of the resonator can be tuned to modulate the direction–dependent polariton–reservoir interaction by adjusting the position of the inner ring while keeping the outer ring fixed. By slightly moving the inner ring position as shown in FIG. 1(b), the condensate transforms from a two-vortex state into a stable single-vortex mode. Our work presents a simple, fully optical method to generate and control vortices in exciton polari-

* tinggegao@tju.edu.cn

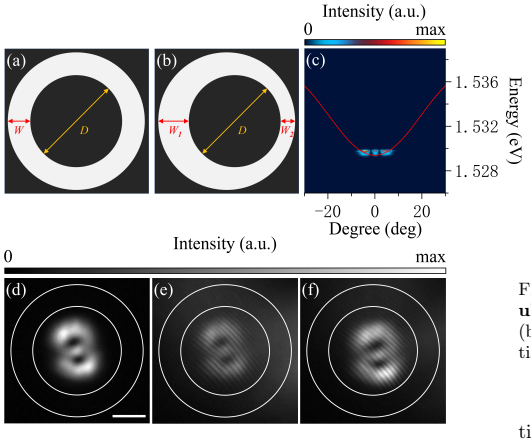

FIG. 1. **Schematic diagram of the pump pattern distribution and the condensation of exciton polaritons in the potential trap.** (a–b) The illustration depicts the potential configurations before and after tuning the pump profile. The pump regions are represented by white rings. (c) The dispersion of the exciton polariton measured above threshold, and the red solid line represents the numerical simulation of the lower polariton branch observed below threshold. (d) Condensed real-space imaging when vortices appear, and the boundaries of the pump region are delineated by white solid circles. (e) Interferometric imaging of the vortices is performed when both carry a topological charge of +1. (f) Interferometric imaging of the vortices is performed when both carry a topological charge of -1. Scale bar: 10 μm.

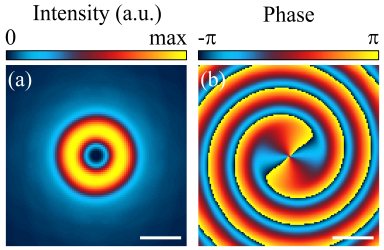

FIG. 2. **A higher-order vortex in the numerical simulation.** (a) Real-space intensity distribution of the vortex. (b) The corresponding phase distribution. No disorder potentials are applied here. Scale bar: 10 μm.

ton condensates by tuning the pumping pattern. Compared with previous work, our approach requires neither electrical tuning nor the complexity of aligning multiple laser beams, while enabling control over both the vortex number and charge [23, 31, 34].

In the experiment, we used a GaAs microcavity, the same as that reported in [35]. The sample is placed in the cryostat at 6±1 K. We used a pump laser operating in continuous-wave mode with a wavelength of 760 nm. The Gaussian beam is first reflected by a DMD, which modulates its spatial geometric shape, then passes through a tubelens and a microscope objective, where it is imaged onto the surface of the microcavity as an annular pattern, and the geometric tuning of the laser pattern configuration is controlled by the DMD. We measured the photoluminescence imaging of exciton polaritons below threshold under the annular patterns, these data are shown in FIG. S1(a) of the Supplementary Material (SM). The real-space images of the condensate and its interference patterns are collected using a Michelson interferometer, where one of the interference beams is amplified to serve as a reference beam, ensuring a smooth phase distribution, and all real-space images were captured with an exposure time of 25 ms. The dispersion is measured by an angle-resolved spectrometer and the dispersion above the threshold is shown in FIG. 1(c), with the pumping densities of 1.5 P_{th}. We also measured the dispersion relation below the threshold at a pumping density of 0.2 P_{th} and fitted the lower branch of the exciton polariton, indicated by the red curve in FIG. 1(c). The detuning of the excited area of the microcavity is around −3.5 meV.

We firstly used a concentric ring-shaped pumping pattern with an inner diameter of $D = 26.8\,\mu$m and an outer ring width of $W = 6.6\,\mu$m, maintaining the pump density at 1.5 P_{th}. In this configuration, two distinct areas of minimal intensity are observed in the exciton polariton condensate (FIG. 1(d)), indicating the existence of two vortices. In order to investigate the phase distribution within the condensate, we performed interferometric measurements on these two vortices using the Michelson interferometer. The interference pattern shows a characteristic fork at each vortex core, with both forks oriented in the same direction (FIG. 1(e–f)). We also extracted the corresponding phase distributions from the interference patterns, the results are presented in FIG. S2(a–b) of the SM. This observation confirms that the condensation contains two vortices with the same topological charge. The micro-defects in the sample lead to the formation of the vortices, whereas the vortex topological charge is determined by the joint contributions from disorder, the subtle gradient ($\sim 1.28 \times 10^{-3}$ meV/μm), polariton–polariton interactions, and the pumping configuration. Notably, the real-space image of the polariton condensate remains stable, whereas the orientation of the forks does change slowly (FIG. 1(d–f)), which is due to the instability of the higher-order vortex originating from the polariton–polariton interaction. In Video S1 of the SM, we provide an experimental video that clearly demonstrates that the orientation of the forks of the two polariton vortices varies randomly within a timescale of

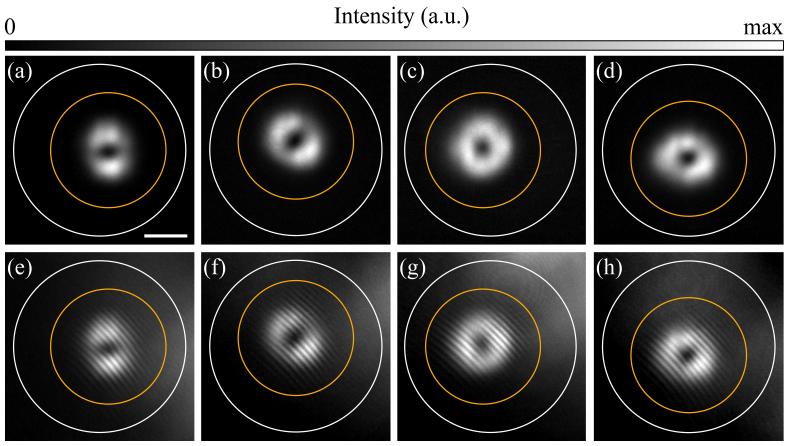

FIG. 3. **The formation of vortices in the exciton polariton condensate under different pumping schemes.** Brown circles denote the displacement of the inner ring in different directions, while the outer ring (white circles) remains fixed. (a–d) Real-space images of the vortices. (e–h) Interferometric imaging with the reference beam corresponding to (a–d), respectively. Scale bar: 10 μm.

several seconds. Although the two forks may occasionally reverse together, their orientations remain consistent.

For a detailed theoretical understanding, the dynamics of polariton condensates can be described by the Gross-Pitaevskii (GP) equation

$$i\hbar\frac{\partial\Psi(\mathbf{r},t)}{\partial t} = \left[-\frac{\hbar^2}{2m}\nabla_\perp^2 - i\hbar\frac{\gamma_c}{2} + g_c|\Psi(\mathbf{r},t)|^2 + \left(g_r + i\hbar\frac{R}{2}\right)n(\mathbf{r},t) + V(\mathbf{r})\right]\Psi(\mathbf{r},t) \quad (1)$$

Here, Ψ is the polariton field. $m = 2\times10^{-4}m_e$ is the effective mass of the condensate with m_e the free electron mass. γ_c=0.1 ps^{-1} represents the loss rate of the condensate and R = 0.01 ps^{-1} μm^2 represents the condensation rate from the exciton reservoir n. The polariton-polariton interaction and polariton-reservoir interaction are denoted by g_c = 5 μeV μm^2 and $g_r = 2g_c$, respectively. $V(\mathbf{r})$ is the potential to characterize the rough surface of the microcavity. The dynamics of the reservoir n satisfy the density equation

$$\frac{\partial n(\mathbf{r},t)}{\partial t} = \left[-\gamma_r - R|\Psi(\mathbf{r},t)|^2\right]n(\mathbf{r},t) + P(\mathbf{r},t)\,. \quad (2)$$

Here, $\gamma_r = 1.5\gamma_c$ is the loss rate of the reservoir and P is the non-resonant pump with a ring shape and the radius of the inner ring and the outer ring of $\sim$7μm and $\sim$12μm, respectively, to keep the vortices in numerical simulations and experiments at a similar size. The difference of the radii of the ring pumps in experiments and numerical simulations is due to the simplified GP model, in which complex relaxation dynamics are neglected. The coupled equations can be solved numerically by using the Runge–Kutta 4th order method [36]. When the inner and outer rings are concentric, the vortex carries a topological charge of +2, see the real-space intensity distribution of the vortex in FIG. 2(a) and its phase profile in FIG. 2(b). Note that here the topological charge is slightly split, i.e., composed of two topological charges of +1 because of the repulsive interaction, although the splitting in the numerical simulation in the current parameter combination is not as obvious as in experiments. Depending on the initial noise conditions, the topological charge of this higher-order vortex can also be −2.

Based on the pumping configuration of FIG. 1(d), we keep the location of the outer ring fixed and gradually move the inner potential trap to the right. This adjustment results in different widths for the potential barriers on the left and right sides, that is, $W_1 > W_2$. The condensation state evolves during the displacement of the inner ring. When W_1 = 8.6 μm and W_2 = 4.6 μm, we observed a single stable vortex in the condensate (FIG. 3(a)). The interferometric image reveals a stable fork, indicating that the vortex has a topological charge of +1 (FIG. 3(e)). Then we move the region of the inner potential trap upward for the same distance, the real-space image shows a similar polariton condensate distribution (FIG. 3(b)), we also observed a single stable vortex and its topological charge is +1, as shown

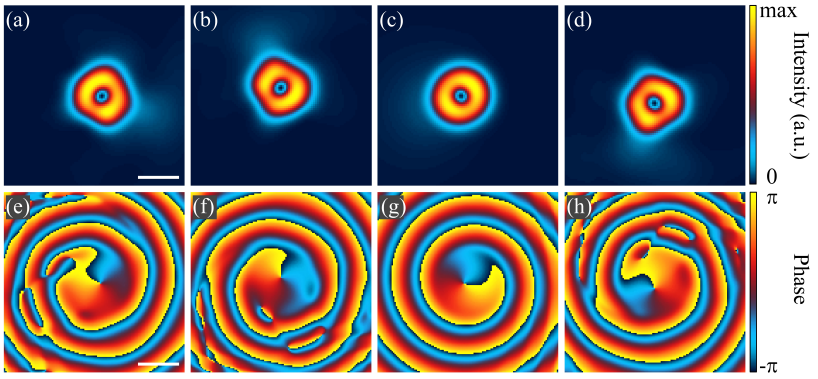

FIG. 4. **Vortices observed in numerical simulations.** (a–d) Real-space intensity distributions of the condensate when the inner ring is tuned along four distinct directions: right, up, left, and down, by 2μm. (e–h) The corresponding phase distributions. Here a disorder potential with the correlation length of $\sim$3 μm and the depth of $\sim$0.2 meV is applied. Scale bar: $10\,\mu$m.

in FIG. 3(f). When the potential trap is moved to the left or downward, the appropriate spatial displacement of the potential trap results in the formation of a stable vortex (FIG. 3(c–d)). However, in contrast to observations above, corresponding to the displacements pointing to the right and upward, here the topological charge of the vortex is reversed from $+1$ to -1 (FIG. 3(g–h)). The photoluminescence imaging below threshold corresponding to the four cases described above are shown in FIG. S1(b–e) of the SM. And the phase distributions around the vortex core for each configuration above are presented in FIG. S2(c–f) of the SM. In experiments, tuning the position of the potential trap can modulate the vortex state by adjusting the spatial distribution of the pump region. Specifically, on the side with a broader pump area (as indicated by W_1 in FIG. 1(b)), the width of the local potential well is larger, while on the side with a narrower pump area (as indicated by W_2 in FIG. 1(b)), the width of the local potential well is smaller. As the spatial displacement of the inner ring area increases, the asymmetry of the pumping pattern becomes increasingly dominant. Furthermore, the direction of displacement of the inner ring area can affect the topological charge of the vortex. As shown in FIG. 3(e–f) and FIG. 3(g–h), the opposite movement of the inner ring area always generates the opposite topological charges.

Defects and other disorder play an important role in the formation of the vortex, but disorder alone is insufficient to control the vortex topological charge. By adjusting the pump profile, we selectively excite vortex states with desired charges, and distinct pumping configurations can thus produce vortices with different topological charges. The topological charge of the vortex induced by the asymmetry of the pumping pattern is stable, and this method of tuning vortex states can be reproduced at another position within the microcavity, as shown in FIG. S3(a–e) of the SM. This confirms that the vortex tuning in our pumping configuration is general and robust.

To demonstrate that, we also simulated the formation dynamics of the vortices by tuning the potential trap in four different directions, the real-space images are shown in FIG. 4(a–d) and the corresponding phase distributions are shown in FIG. 4(e–h). In all four directions, an appropriate displacement of the inner ring can reduce the topological charge of the vortex from 2 to either $+1$ or -1. The displacements of the inner ring in the right and upward directions resulted in the generation of a stable vortex with a topological charge of $+1$ (FIG. 4(e–f)), while the displacements in the left and downward directions induced the formation of a vortex with a topological charge of -1 (FIG. 4(g–h)). Here, we consider a disorder potential $V(\mathbf{r})$ in the simulations to agree with the experimental observations.

Further tuning the region of the potential trap away reduces the stability of the vortex state, leading to its disappearance and eventual replaced by a dipole mode. The real-space images of the dipole modes are plotted in FIG. 5(a–d). In FIG. 5(a), $W_1 = 10.6\,\mu$m and $W_2 = 2.6\,\mu$m, and in the other three directions, the potential trap is moved by the same distance (FIG. 5(b–d)).

In summary, our experimental results reveal that variations in the configuration of the pumping pattern significantly influence exciton polariton condensation. By

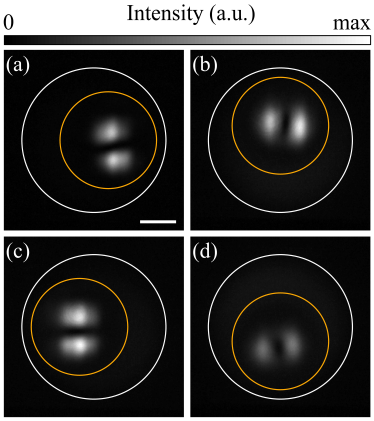

FIG. 5. **The formation of the dipole mode in the exciton polariton condensate when the region of the potential trap is tuned away by a significant distance.** Brown circles denote the displacement of the inner ring in different directions, while the outer ring (white circles) remains fixed. (a–d) Real-space images of the dipole modes when the inner ring is tuned along four distinct directions: right, up, left, and down, by 4μm. Scale bar: 10 μm.

employing an appropriately sized annular potential trap, exciton polariton vortices can be induced. Furthermore, the displacement of the inner ring can enhances the asymmetry of the excitation pattern, thereby generating a stable vortex state. The topological charge of the vortex can be precisely controlled by the direction of movement of the inner ring. And the experimental results are in agreement with the theoretical simulations performed using the GP equation. Our study demonstrates that a straightforward optical method can be used to create and manipulate vortices in exciton polariton condensates.

SUPPLEMENTARY MATERIAL

See the Supplementary Material for additional details on the real-space photoluminescence of exciton polaritons measured below threshold; phase distributions around the vortex core; experimental video of random variation in vortex topological charges; and interferometric imaging at an alternative sample position.

ACKNOWLEDGMENTS

TG acknowledges the support from the National Natural Science Foundation of China (NSFC, No. 12174285). The Paderborn group acknowledges the support from the Deutsche Forschungsgemeinschaft (DFG) (Grant No. 467358803 and No. 519608013) and by Paderborn Center for Parallel Computing, PC^2.

The data that support the findings of this study are available from the corresponding author upon reasonable request.

[1] N. D. Mermin, The topological theory of defects in ordered media, Reviews of Modern Physics **51**, 591 (1979).
[2] G. Tosi, G. Christmann, N. Berloff, P. Tsotsis, T. Gao, Z. Hatzopoulos, P. Savvidis, and J. Baumberg, Geometrically locked vortex lattices in semiconductor quantum fluids, Nature Communications **3**, 1243 (2012).
[3] K. A. Sitnik, S. Alyatkin, J. D. Töpfer, I. Gnusov, T. Cookson, H. Sigurdsson, and P. G. Lagoudakis, Spontaneous formation of time-periodic vortex cluster in nonlinear fluids of light, Physical Review Letters **128**, 237402 (2022).
[4] S. Alyatkin, C. Milián, Y. V. Kartashov, K. A. Sitnik, I. Gnusov, J. D. Töpfer, H. Sigurðsson, and P. G. Lagoudakis, Antiferromagnetic ising model in a triangular vortex lattice of quantum fluids of light, Science Advances **10**, eadj1589 (2024).
[5] R. Panico, P. Comaron, M. Matuszewski, A. Lanotte, D. Trypogeorgos, G. Gigli, M. D. Giorgi, V. Ardizzone, D. Sanvitto, and D. Ballarini, Onset of vortex clustering and inverse energy cascade in dissipative quantum fluids, Nature Photonics **17**, 451 (2023).
[6] J. Wang, Y. Peng, H. Xu, J. Feng, Y. Huang, J. Wu, T. C. Liew, and Q. Xiong, Controllable vortex lasing arrays in a geometrically frustrated exciton–polariton lattice at room temperature, National Science Review **10**, nwac096 (2023).
[7] K. W. Madison, F. Chevy, W. Wohlleben, and J. Dalibard, Vortex formation in a stirred bose-einstein condensate, Physical Review Letters **84**, 806 (2000).
[8] Y. Nagai, Y. Ota, and M. Machida, Inverse coherence effects in nuclear magnetic relaxation rates as a sign of topological superconductivity, Physical Review B **92**, 180502 (2015).
[9] G. Blatter, M. V. Feigel'man, V. B. Geshkenbein, A. I. Larkin, and V. M. Vinokur, Vortices in high-temperature superconductors, Reviews of Modern Physics **66**, 1125 (1994).
[10] J. M. Kosterlitz and D. J. Thouless, Ordering, metastability and phase transitions in two-dimensional systems, Journal of Physics C: Solid State Physics **6**, 1181 (1973).
[11] K. G. Lagoudakis, M. Wouters, M. Richard, A. Baas, I. Carusotto, R. André, L. S. Dang, and B. Deveaud-Plédran, Quantized vortices in an exciton–polariton condensate, Nature Physics **4**, 706 (2008).
[12] A. Kavokin, T. C. Liew, C. Schneider, P. G. Lagoudakis, S. Klembt, and S. Hoefling, Polariton condensates for classical and quantum computing, Nature Reviews Physics **4**, 435 (2022).
[13] Y. Xue, I. Chestnov, E. Sedov, E. Kiktenko, A. K. Fedorov, S. Schumacher, X. Ma, and A. Kavokin, Split-ring polariton condensates as macroscopic two-level quantum systems, Physical Review Research **3**, 013099 (2021).
[14] J. Barrat, A. F. Tzortzakakis, M. Niu, X. Zhou, G. G.

Paschos, D. Petrosyan, and P. G. Savvidis, Qubit analog with polariton superfluid in an annular trap, Science Advances **10**, eado4042 (2024).
[15] T. Hyart, B. van Heck, I. C. Fulga, M. Burrello, A. R. Akhmerov, and C. W. J. Beenakker, Flux-controlled quantum computation with majorana fermions, Physical Review B **88**, 035121 (2013).
[16] M. Mirhosseini, O. S. Magaña-Loaiza, M. N. O'Sullivan, B. Rodenburg, M. Malik, M. P. Lavery, M. J. Padgett, D. J. Gauthier, and R. W. Boyd, High-dimensional quantum cryptography with twisted light, New Journal of Physics **17**, 033033 (2015).
[17] D. Freilich, D. Bianchi, A. Kaufman, T. Langin, and D. Hall, Real-time dynamics of single vortex lines and vortex dipoles in a bose-einstein condensate, Science **329**, 1182 (2010).
[18] X. Ma, C. J. O. Reichhardt, and C. Reichhardt, Manipulation of individual superconducting vortices and stick-slip motion in periodic pinning arrays, Physical Review B **97**, 214521 (2018).
[19] D. N. Krizhanovskii, D. M. Whittaker, R. A. Bradley, K. Guda, D. Sarkar, D. Sanvitto, L. Vina, E. Cerda, P. Santos, K. Biermann, R. Hey, and M. S. Skolnick, Effect of interactions on vortices in a nonequilibrium polariton condensate, Physical Review Letters **104**, 126402 (2010).
[20] C. Weisbuch, M. Nishioka, A. Ishikawa, and Y. Arakawa, Observation of the coupled exciton-photon mode splitting in a semiconductor quantum microcavity, Physical Review Letters **69**, 3314 (1992).
[21] A. V. Kavokin, J. J. Baumberg, G. Malpuech, and F. P. Laussy, *Microcavities* (Oxford University Press, 2017).
[22] Y. Li, X. Ma, X. Zhai, M. Gao, H. Dai, S. Schumacher, and T. Gao, Manipulating polariton condensates by rashba-dresselhaus coupling at room temperature, Nature Communications **13**, 3785 (2022).
[23] X. Zhai, X. Ma, Y. Gao, C. Xing, M. Gao, H. Dai, X. Wang, A. Pan, S. Schumacher, and T. Gao, Electrically controlling vortices in a neutral exciton-polariton condensate at room temperature, Physical Review Letters **131**, 136901 (2023).
[24] J. Kasprzak, M. Richard, S. Kundermann, A. Baas, P. Jeambrun, J. M. J. Keeling, F. Marchetti, M. Szymańska, R. André, J. a. Staehli, *et al.*, Bose–einstein condensation of exciton polaritons, Nature **443**, 409 (2006).
[25] R. Balili, V. Hartwell, D. Snoke, L. Pfeiffer, and K. West, Bose-einstein condensation of microcavity polaritons in a trap, Science **316**, 1007 (2007).
[26] T. Byrnes, N. Y. Kim, and Y. Yamamoto, Exciton–polariton condensates, Nature Physics **10**, 803 (2014).
[27] M. Pieczarka, E. Estrecho, S. Ghosh, M. Wurdack, M. Steger, D. W. Snoke, K. West, L. N. Pfeiffer, T. C. H. Liew, A. G. Truscott, and E. A. Ostrovskaya, Topological phase transition in an all-optical exciton-polariton lattice, Optica **8**, 1084 (2021).
[28] T. Gao, O. A. Egorov, E. Estrecho, K. Winkler, M. Kamp, C. Schneider, S. Höfling, A. G. Truscott, and E. A. Ostrovskaya, Controlled ordering of topological charges in an exciton-polariton chain, Physical Review Letters **121**, 225302 (2018).
[29] C. Schneider, K. Winkler, M. D. Fraser, M. Kamp, Y. Yamamoto, E. Ostrovskaya, and S. Höfling, Exciton-polariton trapping and potential landscape engineering, Reports on Progress in Physics **80**, 016503 (2016).
[30] X. Ma, Y. V. Kartashov, T. Gao, L. Torner, and S. Schumacher, Spiraling vortices in exciton-polariton condensates, Physical Review B **102**, 045309 (2020).
[31] X. Ma, B. Berger, M. Aßmann, R. Driben, T. Meier, C. Schneider, S. Höfling, and S. Schumacher, Realization of all-optical vortex switching in exciton-polariton condensates, Nature Communications **11**, 897 (2020).
[32] T. Gao, G. Li, E. Estrecho, T. C. H. Liew, D. Comber-Todd, A. Nalitov, M. Steger, K. West, L. Pfeiffer, D. W. Snoke, A. V. Kavokin, A. G. Truscott, and E. A. Ostrovskaya, Chiral modes at exceptional points in exciton-polariton quantum fluids, Physical Review Letters **120**, 065301 (2018).
[33] A. V. Yulin, A. S. Desyatnikov, and E. A. Ostrovskaya, Spontaneous formation and synchronization of vortex modes in optically induced traps for exciton-polariton condensates, Physical Review B **94**, 134310 (2016).
[34] N. Carlon Zambon, P. St-Jean, M. Milićević, A. Lemaître, A. Harouri, L. Le Gratiet, O. Bleu, D. Solnyshkov, G. Malpuech, I. Sagnes, *et al.*, Optically controlling the emission chirality of microlasers, Nature Photonics **13**, 283 (2019).
[35] Y. Li, X. Ma, Z. Hatzopoulos, P. G. Savvidis, S. Schumacher, and T. Gao, Switching off a microcavity polariton condensate near the exceptional point, ACS Photonics **9**, 2079 (2022).
[36] J. Wingenbach, D. Bauch, X. Ma, R. Schade, C. Plessl, and S. Schumacher, Phoenix–paderborn highly optimized and energy efficient solver for two-dimensional nonlinear schrödinger equations with integrated extensions, Computer Physics Communications **315**, 109689 (2025).